AIP | Applied Physics Letters

Field-induced defect morphology in Ni-gate AlGaN/GaN high electron mobility transistors

M. R. Holzworth, N. G. Rudawski, P. G. Whiting, S. J. Pearton, K. S. Jones et al.

Citation: Appl. Phys. Lett. **103**, 023503 (2013); doi: 10.1063/1.4813535
View online: http://dx.doi.org/10.1063/1.4813535
View Table of Contents: http://apl.aip.org/resource/1/APPLAB/v103/i2
Published by the AIP Publishing LLC.

Field-induced defect morphology in Ni-gate AlGaN/GaN high electron mobility transistors

M. R. Holzworth,[1,a)] N. G. Rudawski,[1] P. G. Whiting,[1] S. J. Pearton,[1] K. S. Jones,[1] L. Lu,[2] T. S. Kang,[2] F. Ren,[2] E. Patrick,[3] and M. E. Law[3]
[1]*Department of Materials Science and Engineering, University of Florida, Gainesville, Florida 32611-6400, USA*
[2]*Department of Chemical Engineering, University of Florida Gainesville, Florida 32611-6400, USA*
[3]*Department of Electrical and Computer Engineering, University of Florida Gainesville, Florida 32611-6400, USA*

(Received 16 February 2013; accepted 29 May 2013; published online 10 July 2013)

AlGaN/GaN high electron mobility transistors were electrically stressed using off-state high reverse gate biases. In devices demonstrating the largest, most rapid decrease in normalized maximum drain current, defects were found at the gate/AlGaN epilayer interface and characterized using high-angle annular dark-field scanning transmission electron microscopy. These defects appear to be a reaction between the Ni layer of the Ni/Au gate metal stack and the AlGaN epilayer. Additionally, simulations of the electric field lines from the defective devices match the defect morphology. These results provide important insight toward understanding failure mechanisms and improving reliability of Ni-gate AlGaN/GaN high electron mobility transistors. © *2013 AIP Publishing LLC*. [http://dx.doi.org/10.1063/1.4813535]

AlGaN/GaN high electron mobility transistors (HEMTs) remain attractive for high frequency, high power, and high temperature applications.[1–8] However, many reliability issues have arisen and have been reported throughout the literature.[9–18] More specifically, physical degradation of the AlGaN epilayer at the edges of the gate contact and interactions between the gate contact metal and epilayers have been observed using transmission electron microscopy (TEM), scanning electron microscopy (SEM), and atomic force microscopy.[18–22] The epilayer degradation near the gate contact, degradation of the Ni/AlGaN interface, and transport of gate metal into the epilayers decreases drain current, which contributes to a reduction in the reliability of the HEMTs.[9,11,18] Understanding the mechanisms behind these interactions could enhance the reliability of AlGaN/GaN HEMTs by circumventing the defect formation conditions and preventing device degradation. Therefore, accurate structural characterization of defects is crucial in understanding the defect formation mechanism(s) and potentially improving HEMT reliability and performance. Here, high-angle annular dark-field scanning TEM (HAADF-STEM) was used to characterize a structural defect that forms between the Ni layer of a Ni/Au gate and the AlGaN epilayer during electrical stressing. It was found that the defect morphology approximates the simulated electric field during device electrical stressing indicating the shape of the field is an important factor influencing defect formation.

The AlGaN/GaN HEMTs used for this work were all grown on the same semi-insulating 6H-SiC substrate and received the same processing. An AlN nucleation layer was used on the SiC and followed by a 2.25 μm-thick Fe-doped GaN buffer, 15 nm of $Al_{0.28}Ga_{0.72}N$, and capped with 3 nm of an unintentionally doped GaN layer (this layer is not normally visible in TEM micrographs). The ohmic contacts consisted of metal stacks of Ti/Al/Ni/Au annealed for 30 s at 850 °C.[13,16,17] Additionally, the gate contact consisted of a Ni/Au metal stack. The devices employed a "double-gate" design with each gate having a 150 μm width and a gate length (L_G) of 100 nm (TEM micrographs indicate $L_G \sim 55$ nm at the Ni/AlGaN interface). Finally, the devices were passivated with SiN_x. A typical cross section of the devices is shown in the HAADF-STEM image presented in Fig. 1, with the source, gate, and drain contacts indicated. The structure of the devices was analyzed using HAADF-STEM performed using a JEOL 2010 F transmission electron microscope operated at 200 kV; samples for HAADF-STEM imaging were prepared via focused ion beam (FIB) milling using an FEI DB235 dual focused ion beam/scanning electron microscope. Electrical data was measured using a HP 4156C semiconductor parameter analyzer (baseline noise level of a few pA). Off-state high reverse gate bias conditions were used to electrically stress nominally identical HEMTs. During the applied stress, a constant drain-source voltage $V_{DS} = 5$ V was applied to each sample. However, the gate-source voltage (V_{GS}) was varied for each sample during stressing and started at either −5 or −10 V and ended at −42 V with the gate voltage stepped at −1 V/min. Thus, the data presented in Fig. 2 are discrete with each data point corresponding to an incremental change in V_{GS} (−1 V); the data points are connected using continuous curves only to aid in viewing general trends. Electrical parameters of each HEMT were measured between each unit decrease in V_{GS} at $V_{DS} = 5$ V and $V_{GS} = 0$ V. All stressing occurred at 25 °C and in ambient atmosphere.

After application of the electrical stress, two different behaviors, "slow" and "rapid" degradation, were observed for the change in normalized maximum drain current ($I_{D\,max}$) of the HEMTs as given by $I_{D\,max}(V_{GS})/I_{D\,max}(0)$, where $I_{D\,max}(V_{GS})$ is the maximum drain current measured after the applied gate stress of V_{GS} and $I_{D\,max}(0)$ is the maximum drain

a)Author to whom correspondence should be addressed. Electronic mail: montaray@ufl.edu

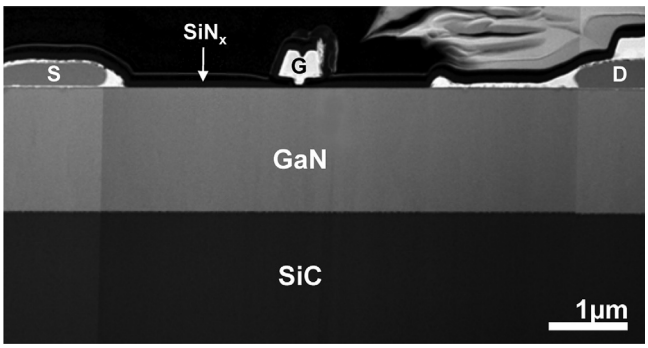

FIG. 1. Low magnification HAADF-STEM image of a cross section of an unstressed AlGaN/GaN HEMT with the source (S), gate (G), and drain (D) contacts labeled.

current of the unstressed device measured before the application of electrical stress. For each device, the applied electrical stress decreases the measured $I_{D\,max}$; therefore, the normalized $I_{D\,max}$ decreases as stressing continues. The first typical behavior of normalized $I_{D\,max}$ is shown by the curve labeled "$I_{D\ slow}$" in Fig. 2 and is observed to be a relatively "slow" degradation process. On average, devices that exhibit this "slow" degradation behavior show a decrease of ~3.5% in normalized $I_{D\,max}$ by $V_{GS} = -22$ V. Furthermore, by the end of stressing at $V_{GS} = -42$ V, normalized $I_{D\,max}$ has decreased on average by ~13 ± 4%. This behavior is in contrast to the second behavior shown by the curve labeled "$I_{D\,rapid}$" presented in Fig. 2, which is characterized as a "rapid" degradation process and occurred in ~14% of HEMTs in this study. For this degradation, the normalized $I_{D\,max}$ has decreased by ~16% by $V_{GS} = -22$ V, which is more than a 350% larger decrease in normalized $I_{D\,max}$ compared to the "slow" degradation process at $V_{GS} = -22$ V. Additionally, by $V_{GS} = -42$ V, normalized $I_{D\,max}$ has decreased by ~26%, which is a decrease in normalized $I_{D\,max}$ of 200% compared to the "slow" degradation process. Finally, it should be noted that the overall decrease in drain current (I_{DS}) was permanent after stressing as revealed by the I_{DS} versus V_{GS} family of curves (not presented) between the "slow" and "rapid" degradation devices measured approximately 48 h after stressing. Furthermore, the permanent decrease in I_{DS} was ~14% ± 4% for the "slow" degradation samples compared to ~37% for the "rapid" degradation sample at $V_{GS} = -2$ V.

Additionally, the gate current (I_G) behaviors between the "slow" and "rapid" degradation HEMTs shown in Fig. 2 are dissimilar. On average for the "slow" HEMTs, "$I_{G\,slow}$" dramatically increases by approximately two orders of magnitude at a lower V_{GS} compared to the "rapid" degradation process indicated by "$I_{G\,rapid}$." Also, for the "slow" HEMTs it is evident that only after the large increase in I_G at $V_{GS} = -14$ V does the normalized $I_{D\,max}$ begin to degrade. Before this large increase in I_G, $I_{D\,max}$ had degraded by <1% over the first 10 V of applied gate stress; however, after the I_G jump, $I_{D\,max}$ degraded slowly and relatively constantly at ~0.5%/V until the end of stressing. This is in contrast to the "rapid" degradation process where $I_{D\,max}$ began to decrease as soon as stressing initiated. This distinction between the characteristic $I_{D\,max}$ and I_G curves of the sets of devices indicates that different degradation modes are occurring.

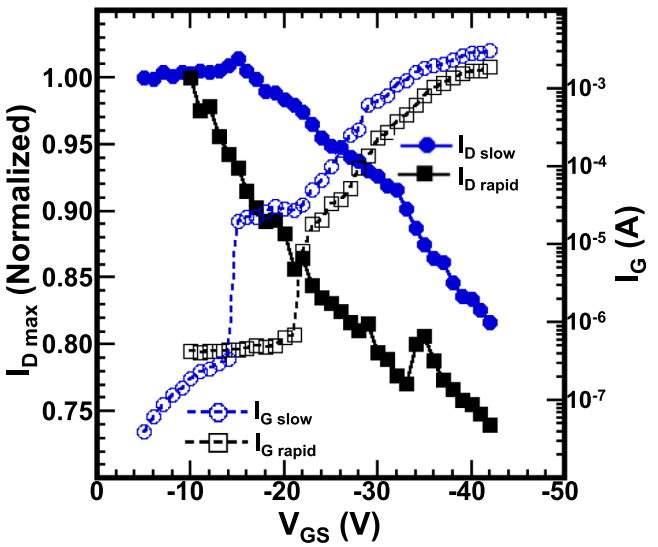

FIG. 2. Measured normalized $I_{D\,max}$ and I_G of characteristic "slow" and "rapid" degradation HEMTs when stressed from $V_{GS} = -5$ or -10 V to -42 V at -1 V/min and V_{DS} maintained at 5 V throughout stressing; continuous curves are shown only to aid in observing general trends in data.

Following the application of electrical stress, the HEMTs were serially sectioned along the width of the gate using site-specific FIB milling. Each sample was serially sectioned at approximately 9–15 locations with the sections approximately 10 μm long by 1 μm wide by 2 μm deep and spaced approximately 10–15 μm apart. From the exposed cross sections, the gates were inspected for defects and irregularities using cross-sectional scanning electron microscopy (XSEM) at an incident angle of 52°. After examining the gate/AlGaN epilayer interface using XSEM, some sections were further thinned for TEM analysis. HAADF-STEM images of typical "slow" and "rapid" degradation samples are presented in Figs. 3(a) and 3(b), respectively. In these images, brighter features correspond to areas of greater average atomic number; the individual Au, Ni, AlGaN, and GaN layers are indicated in Fig. 3(a).

The "slow" degradation HEMT, shown in Fig. 3(a), shows no obvious physical degradation and the gate contact has maintained the same morphology as the unstressed control HEMT shown at lower magnification in Fig. 1. Furthermore, no defects were ever observed in any of the "slow" degradation samples. However, the gate region of a "rapid" degradation HEMT exhibits a markedly different morphology as shown in Fig. 3(b). This image indicates the presence of an "arch"-shaped defect under the gate, which penetrates into the AlGaN epilayer at two points. Although this defect penetrates the AlGaN epilayer, it stops before crossing the AlGaN/GaN interface. However, the presence of this defect near the interface may still impact the electrical performance of the device possibly by influencing leakage and/or trapping, and it may explain the rapid decrease in normalized $I_{D\,max}$ compared to "slow" degradation devices that exhibited no early, rapid decrease in normalized $I_{D\,max}$ and no observed defect formation. It should be noted that this defect was present throughout the entire device width and corresponds to the $I_{D\ rapid}$ and $I_{G\,rapid}$ curves shown in Fig. 2 indicating the largest initial drop in normalized $I_{D\,max}$. Additionally, I_G is greater in the

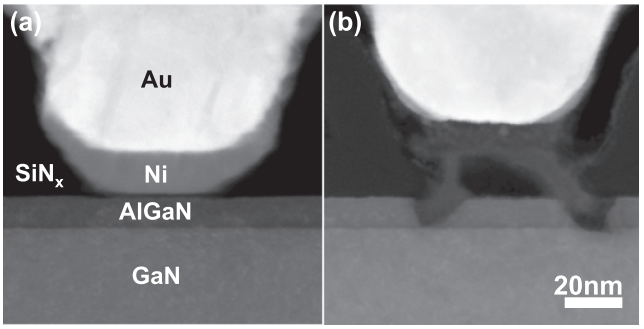

FIG. 3. High magnification HAADF-STEM images of the gate region of AlGaN/GaN HEMTs showing the distinct gate metal stack layers and semiconducting epilayers in (a) devices experiencing "slow" degradation, which are basically indistinguishable from unstressed devices and (b) in devices experiencing "rapid" degradation showing an "arch"-shaped defect formed from the original Ni layer of the gate and penetrating into the AlGaN epilayer.

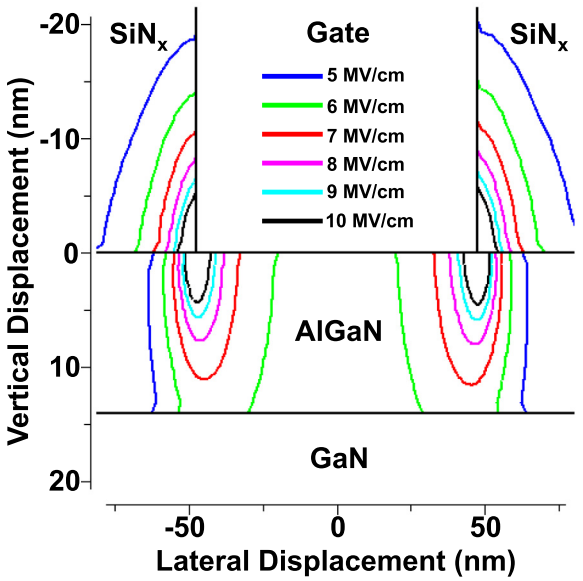

FIG. 4. Simulation showing the iso-contour lines of the magnitude of the vertical and lateral components of the electric field in a "rapid" degradation HEMT at a stress state of $V_{DS} = 5$ V and $V_{GS} = -42$ V.

"slow" degradation HEMTs showing no physical degradation compared to the "rapid" degradation, which contain physical defects indicating that $I_{D\,max}$ is a more useful measure of physical device degradation. Furthermore, this pattern of an initial "rapid" degradation in $I_{D\,max}$ has been observed in multiple HEMTs spanning different starting V_{DS} (not shown here) containing physical defects compared to devices that show "slow" degradation and no defects. Finally, the bottom of the Au layer of the gate is elevated relative to the AlGaN layer in "rapid" degradation HEMT, indicating that the defect formation pushed the gate vertically from its initial position and partially separated it from the SiN_x passivation.

Additionally, energy dispersive X-ray spectroscopy (EDS) and electron energy-loss spectroscopy (EELS) analyses were performed on the "arch"-shaped defect (not presented) suggesting the defect region contains Al, Ga, Ni, and O but not N; a more detailed analysis of the chemistry of the defect will be presented in a subsequent paper. These preliminary EDS and EELS works are consistent with the HAADF-STEM image of Fig. 3(b), in which the contrast mechanism arises from differences in the average atomic number. In general, the defect is darker in contrast than both the Ni and the AlGaN epilayer. This implies that there was a decrease in average atomic number, which is consistent with the EDS and EELS results showing the presence of O in the defect.

In order to better understand the change in shape of the gate upon degradation, a simulation of the electric field in the "rapid" degradation process was performed using the Florida Object Oriented Device Simulator.[23,24] Measured electrical data were used to calibrate the simulated results to actual device performance, and no temperature effects were taken into account in the simulation due to the off-state stress where there should be negligible current flow and heating. At approximately $V_{GS} = -23$ V, $I_{G\,rapid}$ has jumped two orders of magnitude, suggesting an electronic or physical leakage path between the two-dimensional electron gas at the AlGaN/GaN interface and gate as shown in Fig. 2; however, $I_{D\ rapid}$ has decreased since the initial application of stress. Therefore, the "arch"-shaped defect shown in Fig. 3(b) could have formed continuously throughout the entire application of electrical stress. Consequently, the electric field is plotted at the final voltage condition, $V_{DS} = 5$ V and $V_{GS} = -42$ V, and is shown in Fig. 4, where iso-contour lines of the magnitude of the vertical and lateral components of the electric field are indicated. It is noted that due to the inverse piezoelectric effect, the electric and strain fields are linked.[25] Therefore, the magnitude of the strain field is proportional to this simulated electric field at these bias conditions and would possess the same shape. Furthermore, it appears the 6 MV/cm contour line approximately models the form of the "arch"-shaped defect, which indicates that the electric/strain field may influence the evolution of defect morphology. Previous work has suggested that defects and reactions occur where the electric field is largest in a HEMT, at the gate edges.[20,26] However, in this case, due to this large, nearly symmetric electric/strain field present, it is possible that the fields influence the diffusion or reactivity of the layers and O directly contributing to the morphology of the defect and explain the similarity between the defect shape and the simulated electric/strain field contours. This could indicate that it is the shape of the electric/strain field itself that influences the defect morphology and not just the large magnitude of the field for HEMTs with $L_G < 100$ nm.

In conclusion, high-angle annular dark-field scanning transmission electron microscopy was used to study a reaction-based defect present between the Ni layer of a Ni/Au gate and the AlGaN epilayer of an AlGaN/GaN high electron mobility transistor. Where the normalized maximum drain current was rapidly and greatly reduced compared to "slow" degrading devices, "arch"-shaped oxidation defects associated with significant reaction between the Ni and AlGaN were observed. This is particularly noticeable during early electrical stressing where the difference between the two sets of devices was greatest. Due to the devices originating from the same wafer with identical processing, the O in the defect likely could have come from the SiN_x passivation or from the ambient after diffusion through the passivation. Additionally, the defect imitates

the shape of the simulated electric/strain field iso-contour at approximately 6 MV/cm present in the device during electrical stressing, suggesting that the shape of the field may influence defect morphology.

The authors acknowledge the Air Force Office of Scientific Research and the Multidisciplinary Research Initiative for funding this research and the Major Analytical Instrumentation Center at the University of Florida for use of the TEM and FIB facilities.

[1]M. Feng, S. Shyh-Chiang, D. C. Caruth, and J. J. Huang, Proc. IEEE **92**, 354 (2004).
[2]Nidhi S. Dasgupta, S. Keller, J. S. Speck, and U. K. Mishra, IEEE Electron Device Lett. **32**, 1683 (2011).
[3]S. Tirelli, D. Marti, H. Sun, A. R. Alt, J.-F. Carlin, N. Grandjean, and C. R. Bolognesi, IEEE Electron Device Lett. **32**, 1364 (2011).
[4]J. W. Johnson, E. L. Piner, A. Vescan, R. Therrien, P. Rajagopal, J. C. Roberts, J. D. Brown, S. Singhal, and K. J. Linthicum, IEEE Electron Device Lett. **25**, 459 (2004).
[5]Y. Hao, L. Yang, X. Ma, J. Ma, M. Cao, C. Pan, C. Wang, and J. Zhang, IEEE Electron Device Lett. **32**, 626 (2011).
[6]W. Nagy, J. Brown, R. Borges, and S. Singhal, IEEE Trans. Microwave Theory Tech. **51**, 660 (2003).
[7]D. Maier, M. Alomari, N. Grandjean, J.-F. Carlin, M.-A. di Forte-Poisson, C. Dua, A. Chuvilin, D. Troadec, C. Gaquiere, U. Kaiser, S. L. Delage, and E. Kohn, IEEE Trans. Device Mater. Reliab. **10**, 427 (2010).
[8]D. Marcon, X. Kang, J. Viaene, M. Van Hove, P. Srivastava, S. Decoutere, R. Mertens, and G. Borghs, Microelectron. Reliab. **51**, 1717 (2011).
[9]U. Chowdhury, J. L. Jimenez, C. Lee, E. Beam, P. Saunier, T. Balistreri, P. Seong-Yong, L. Taehun, J. Wang, M. J. Kim, J. Jungwoo, and J. A. del Alamo, IEEE Electron Device Lett. **29**, 1098 (2008).
[10]J. Jungwoo and J. A. del Alamo, IEEE Electron Device Lett. **29**, 287 (2008).
[11]S. Y. Park, C. Floresca, U. Chowdhury, J. L. Jimenez, C. Lee, E. Beam, P. Saunier, T. Balistreri, and M. J. Kim, Microelectron. Reliab. **49**, 478 (2009).
[12]A. del Alamo and J. Joh, Microelectron. Reliab. **49**, 1200 (2009).
[13]C.-Y. Chang, T. Anderson, J. Hite, L. Lu, C.-F. Lo, B.-H. Chu, D. J. Cheney, E. A. Douglas, B. P. Gila, F. Ren, G. D. Via, P. Whiting, R. Holzworth, K. S. Jones, S. Jang, and S. J. Pearton, J. Vac. Sci. Technol. B **28**, 1044 (2010).
[14]M. R. Holzworth, N. G. Rudawski, S. J. Pearton, K. S. Jones, L. Lu, T. S. Kang, F. Ren, and J. W. Johnson, Appl. Phys. Lett. **98**, 122103 (2011).
[15]M. Kuball, M. Tapajna, R. J. T. Simms, M. Faqir, and U. K. Mishra, Microelectron. Reliab. **51**, 195 (2011).
[16]E. A. Douglas, C. Y. Chang, D. J. Cheney, B. P. Gila, C. F. Lo, L. Lu, R. Holzworth, P. Whiting, K. Jones, G. D. Via, J. Kim, S. Jang, F. Ren, and S. J. Pearton, Microelectron. Reliab. **51**, 207 (2011).
[17]E. A. Douglas, C. Y. Chang, B. P. Gila, M. R. Holzworth, K. S. Jones, L. Liu, J. Kim, S. Jang, G. D. Via, F. Ren, and S. J. Pearton, Microelectron. Reliab. **52**, 23 (2012).
[18]P. G. Whiting, N. G. Rudawski, M. R. Holzworth, S. J. Pearton, K. S. Jones, L. Liu, T. S. Kang, and F. Ren, Microelectron. Reliab. **52**, 2542 (2012).
[19]P. Makaram, J. Joh, J. A. del Alamo, T. Palacios, and C. V. Thompson, Appl. Phys. Lett. **96**, 233509 (2010).
[20]F. Gao, B. Lu, L. Li, S. Kaun, J. S. Speck, C. V. Thompson, and T. Palacios, Appl. Phys. Lett. **99**, 223506 (2011).
[21]L. Li, J. Joh, J. A. del Alamo, and C. V. Thompson, Appl. Phys. Lett. **100**, 172109 (2012).
[22]M. R. Johnson, D. A. Cullen, L. Liu, T. S. Kang, F. Ren, C.-Y. Chang, S. J. Pearton, S. Jang, J. W. Johnson, and D. J. Smith, J. Vac. Sci. Technol. B. **30**, 062204 (2012).
[23]M. Liang and M. E. Law, IEEE Trans. Comput.-Aided Des. **13**, 1235 (1994).
[24]M. E. Law and S. M. Cea, Comput. Mater. Sci. **12**, 289 (1998).
[25]J. Curie and P. Curie, C. R. Acad. Sci. Hebd Seances Acad. Sci. D **91**, 249 (1880), available at: http://visualiseur.bnf.fr/Visualiseur?O=NUMM-3048&I=296&M=tdm.
[26]S. D. Burnham, R. Bowen, P. Willadsen, H. Bracamontes, P. Hashimoto, M. Hu, D. Wong, M. Chen, and M. Micovic, Phys. Status Solidi C **8**, 2399 (2011).